On-chip topological beamformer for multi-link terahertz 6G to XG wireless

Wenhao Wang[1,2], Yi Ji Tan[1,2], Thomas CaiWei Tan[1,2], Abhishek Kumar[1,2], Prakash Pitchappa[3], Pascal Szriftgiser[4], Guillaume Ducournau[5] and Ranjan Singh[1,2,*]

[1]Division of Physics and Applied Physics, School of Physical and Mathematical Sciences, Nanyang Technological University, Singapore 637371, Singapore

[2]Centre for Disruptive Photonic Technologies, The Photonics Institute, Nanyang Technological University, Singapore 637371, Singapore

[3]Institute of Microelectronics, Agency for Science, Technology and Research, Singapore 138634, Singapore

[4]Laboratoire de Physique des Lasers, Atomes et Molécules, PhLAM, UMR 8523 Université de Lille, CNRS, 59655 Villeneuve d'Ascq, France

[5]Université de Lille, CNRS, Centrale Lille, Univ. Polytechnique Hauts-de-France, UMR 8520, IEMN—Institut d'Electronique de Microélectronique et de Nanotechnologie, Lille, France

[*]Email: ranjans@ntu.edu.sg

Terahertz (THz) wireless communication holds immense potential to revolutionize future 6G to XG networks with high capacity, low latency, and extensive connectivity. Efficient THz beamformers are essential for energy-efficient connections, compensating path loss, optimizing resource usage, and enhancing spectral efficiency. However, current beamformers face challenges including significant loss, limited bandwidth, constrained spatial coverage, and poor integration with on-chip THz circuits. We present an on-chip broadband THz topological beamformer using valley vortices for waveguiding, splitting, and perfect isolation in waveguide phased arrays, featuring 184 densely packed valley-locked waveguides, 54 power splitters, and 136 sharp bends. Leveraging neural network-assisted inverse design, the beamformer achieves complete 360° azimuthal beamforming with gains of up to 20 dBi, radiating THz signals into free space with customizable user-defined beams. Photoexciting the all-silicon beamformer enables reconfigurable control of THz beams. The low-loss and broadband beamformer enables a 72 Gbps chip-to-chip wireless link over 300 mm and eight simultaneous 40 Gbps wireless links. Using four of these links, we demonstrate point-to-4-point real-time HD video streaming. Our work provides a complementary metal-oxide-semiconductor (CMOS) compatible THz topological photonic integrated circuit for efficient large-scale beamforming, enabling massive single-input multiple-output (SIMO) and multiple-input and multiple-output (MIMO) systems for terabit-per-second 6G to XG wireless communications.

Advanced Mobile Phone System (AMPS) by Bell Labs in the 1980s ushered in the first-generation (1G) network, initiating the wireless communication. Over four decades, cellular networks evolved to the fifth-generation (5G) driven by the ever-increasing demand for wireless links with large capacity, low latency, and high security[1]. Terahertz band (0.1-10 THz) is promising to achieve Terabit-per-second (Tbps) wireless links for the future sixth generation (6G) and beyond (XG) communication[2-7]. However, the wireless transmission of THz waves suffers from atmospheric attenuation and high propagation loss. The atmospheric window around 300 GHz can be utilized to minimize the attenuation (< 10 $dB.km^{-1}$)[5] and design highly directional antennas to compensate for the free-space path loss. In addition, to extend the spatial coverage of the signal transmission and increase the spectral efficiency, beam steering and beamforming are indispensable to directionally transmit the THz signal towards spatially separated users[8-10], enabling massive single-input multiple-output (SIMO) and multiple-input and multiple-output (MIMO) systems for 6G to XG wireless communications.

Efficient THz beamforming with low power loss, large spectral bandwidth, compact device design, and large spatial tuning range of radiating beams has been a long-standing challenge. Among the various THz beamforming strategies like using reconfigurable diffractive structures and implementing frequency scanning on dispersive structures, the use of phased array is the predominant approach[8,9]. However,

it is challenging to achieve THz beam steering over a large aperture size of several centimeters using electronic[11,12] or photonic[13] active phased arrays due to the sophisticated architectures[14]. It is even more challenging to use them for the receiver (Rx) front-ends[9]. Passive phased array, consisting of a single transmitter (Tx) linked to a compact THz phase shifter network, could mitigate these challenges. Yet low-loss and broadband THz phase shifter is elusive, and the spatial steering range is limited. Moreover, integrating passive phased arrays into on-chip THz-wave integrated circuits is challenging due to their dependence on coupling free-space plane waves.

Valley photonic crystals (VPCs) has recently emerged as a powerful platform for integrated micro-nano photonics due to its capacity to robustly transport light[15-22]. Here we demonstrate an on-chip multi-link THz topological beamformer based on the topological valley photonics-empowered waveguide phased arrays, which directionally transmit the on-chip THz signal into free space with desired number of beams at arbitrary azimuthal angles. The valley vortices enable the robust propagation and splitting of THz waves, and effectively suppress crosstalk between neighboring radiating channels of the topological waveguide phased arrays. With the aid of neural network (NN)-assisted inverse design, we realize complete 360° azimuthal beamforming and achieve a maximum gain of 20 dBi. We further demonstrate reconfigurable beam switching and control over the number of THz beams by photoexciting the silicon-VPC chip. Using a pair of topological beamformers as both

Tx and Rx, we achieve 72 Gbit/s chip-to-chip wireless communication over 300 mm. We also realize eight simultaneous 40 Gbit/s THz wireless communication links, each with distinct azimuthal angles. Among these, we select four beams to showcase real-time streaming of uncompressed HD video in a point-to-4-point setup.

Results

The topological beamformer is fabricated on high resistive silicon wafer (see Methods for the details of fabrication). The VPC has a honeycomb lattice (lattice constant a = 242.5 μm) and a rhombus unit cell, consisting of two equilateral triangular air holes with a side length of l_1 and l_2, respectively (Fig. 1b). The VPC unit cells are categorized into Type A ($l_1 = 0.65a > l_2 = 0.35a$) and Type B ($l_1 = 0.35a < l_2 = 0.65a$) unit cells. When a THz signal is coupled to the topological chip through a taper, it is guided by the valley-locked waveguides, split several times through the topological power splitters, and channeled into six major branches, each separated by 60° in azimuth (Fig. 1a). At each branch, the THz wave is further split three times by a 3-stage power splitter. Finally, the taper array transmits the on-chip THz signal into free space with different number of THz beams having desired azimuthal angles. The topological beamformers are classified as AB-type and BA-type according to the interfacial waveguides that the taper arrays are integrated with (Fig. 1b). Using a fully connected NN-assisted inverse design, the spatial phase profiles of taper arrays are predicted and patterned by changing the length of tapers, leading to the desired radiation pattern. Each AB- (BA-) type

topological beamformer provides a desired number of wireless links at arbitrary azimuthal angles within a range of 94° (66°) for a carrier frequency f_c = 0.325 THz (Fig. 1c). Hence, the topological chip consisting of three AB-type and three BA-type beamformers could realize 360° full azimuthal beamforming. Through optical pumping of the silicon chip, the entire communication channel of the target link can be switched-off, effectively serving as a broadband reconfigurable beamformer.

Design of topological beamformers

When the inversion symmetry is preserved ($l_1 = l_2$), the VPC exhibits C_6 symmetry leading to a pair of degenerate Dirac points at K and K' valleys (Fig. 2a). Breaking the inversion symmetry ($l_1 \neq l_2$) opens the topological bandgaps at K and K' valleys. Type A and Type B unit cells exhibit opposite Poynting vector flow vortices (Fig. 2b), signifying support for opposite rotating states. The calculated Berry curvature localized around K and K' valleys with opposite signs, indicate opposite signed valley Chern numbers which characterize the topological phase of VPCs. Since Type A and Type B unit cells have different topological phases, interfacing them gives rise to a pair of topological edge states due to bulk-boundary correspondence (Fig. 2c)[23]. At K valley, Type A (B) VPC unit cell supports a clockwise (anti-clockwise) Poynting vector flow vortex. Due to vortex matching, AB-type (BA-type) zigzag interface supports a forward (backward) propagating edge state at K valley (see details in Supplementary Section 1). The valley-vortices robustly guide the THz wave transport through sharp corners

123 having bending radius r = 0 μm (Figs. 2d-(i) and 2e-(i)) with a bending loss < 0.1 dB
124 per bend[21].
125
126 Efficient power splitter is essential for the configuration of 1-to-2^n phased arrays. The
127 four-channel (4-CH) AB-type power splitter is composed of an AB-type zigzag
128 interface on the left channel CH 1 and three BA-type zigzag interfaces on the right
129 channels CHs 2-4 (Fig. 2d-e-(ii) and Extended Data Fig. 1). When the THz wave is
130 incident into CH 1, it couples to the forward propagating edge state at K valley. Due to
131 valley locking and vortex matching, the wave is equally split at the intersection and
132 coupled only into CH 2 and CH 3. See Supplementary Section 2 for BA-type
133 topological power splitter. Perfect channel isolation is another critical requisite for
134 phased arrays. The opposing vortices flanking the central interface yield opposite
135 vertical (y) Poynting vector components in adjacent channels (Fig. 2e-(iii)). Their
136 destructive interference results in zero power flow across the interface, ensuring
137 channel isolation in the topological waveguide phased arrays.
138
139 Due to the odd (even) nature of AB-type (BA-type) edge state, asymmetric (symmetric)
140 structural configuration is applied to integrate the taper into the topological interface
141 (Supplementary Section 3). Fig. 2f shows the simulated magnetic field $|H_z|$ distribution
142 in an AB-type 4-stage beamformer which has 2^4 = 16 radiating channels
143 (Supplementary Videos SV1). Owing to the low bending and splitting losses in the

topological chip, the maximum transmission remains at -0.96 dB and the 3-dB bandwidth is 25.4 GHz even when the channel number increases to 64 (Fig. 2g). The measured transmission of the 0-stage chip having only one output taper has a similar bandwidth, but the transmission band shifts to the higher frequency by 10 GHz due to the different thickness of the fabricated VPC chip (Supplementary Section 6). The BA-type beamformers have similar transmission with a measured bandwidth of 28 GHz (Extended Data Fig. 2).

Fig. 3a shows the optical image of an AB-type 4-stage beamformer. See Extended Data Fig. 3 for the evolution of AB-type beamformer from 0-stage to 4-stage. The 16 channels have similar transmission while exhibiting a π phase difference between the neighboring channels due to the odd nature of AB-type edge state. It demonstrates that the AB-type beamformer is an intrinsic broadband phased array (Extended Data Fig. 2). The steering angle θ of a planar one-dimensional (1D) phased array is given by:

$$\sin\theta = \frac{\varphi}{2\pi}\frac{\lambda}{d}, \quad (1)$$

where φ is the phase increment, λ is the free-space wavelength, and d is the distance between the neighboring channels. For intrinsic AB-type topological beamformers, φ is $\pm\pi$ and d is 630 μm, so the azimuthal steering angle θ is ±45.9° at 0.331 THz. Two main lobes with a curved fan shape are observed at θ = -46° and 47° in the horizontal plane (polar angle ϕ = 0°) in the measured three-dimensional (3D) radiation pattern at 0.331 THz (Fig. 3b). Additionally, the radiation extends vertically from ϕ = -30° to 30°.

Broadband beamforming is successfully achieved over a range of 30 GHz, with the steering angle changing slightly from $\theta = \pm 49°$ at 0.31 THz to $\pm 44°$ at 0.34 THz (Fig. 3c). A high gain of 16 dBi is obtained across the entire bandwidth, with the main lobes having 3-dB angular widths of 6.2° and 5.7°. See Extended Data Fig. 4 for the evolution of the radiation pattern of intrinsic AB-type beamformers with varying stage numbers. In the intrinsic BA-type beamformer where $\varphi = 0$ (Fig. 3d), all power is directed towards $\theta = 0°$ across the entire 28 GHz bandwidth (Fig. 3f). The measured peak gain is 20 dBi with a 3-dB azimuthal angular width of 3°.

We adjust the length L of the taper coupler to attain precise 2π-phase control while maintaining the transmission for each radiating channel of the topological beamformer (Extended Data Fig. 5). NN-assisted inverse design is applied to predict the spatial distributions of L, which correspond to the phase profiles of the topological beamformer (Supplementary Section 7). Displayed in Fig. 3g, the radiated THz beam is spatially tailored, generating three to eight lobes with adaptable azimuthal angles covering a broad span of 91.8° at 0.331 THz and across the entire 30 GHz bandwidth (see Extended Data Fig. 6).

Phototunable 360° topological beamformer

BA-type topological beamformers are engineered to radiate THz beam within an azimuthal angle range of 65.2° at 0.331 THz (Supplementary Section 7) due to the

larger d = 840 μm. A 360° full azimuthal beamformer was designed by integrating three AB and three BA-type 3-stage beamformers into a single chip (Fig. 1a). In AB-type beamformers, the lengths of the tapers are adjusted, whereas in BA-type beamformers, all tapers maintain uniform length to emit a single THz beam at each branch. Five lobes separated by 60° in azimuth are measured throughout the entire bandwidth of 28 GHz (Fig. 3i). Each lobe has a clear fan shape with the radiation spanning in the vertical direction from ϕ = -30° to 30° (Supplementary Section 8).

We actively control the 360° radiation pattern of the beamformer by photoexciting the silicon VPC chip with a 525 nm continuous wave laser. When Pump1 is on (Fig. 3h), all five beams across the entire bandwidth are switched off with a substantial gain modulation of ≥ 9.4 dB (Fig. 3i). Alternatively, the single THz beam radiated by the B4 branch is switched off by Pump2 with a gain modulation of 9.6 dB. See Methods for the detailed discussion about the phototunable 360° topological beamformer.

Chip-to-chip THz wireless

The topological beamformers serve as both Txs and Rxs due to their passive architecture. We perform chip-to-chip THz wireless communication experiments using a pair of intrinsic AB-type 4-stage topological beamformers (Fig. 4a and Methods). The group delay is nearly constant within the transmission band (Fig. 4b), which originates from the linear dispersion of the edge states. The radiated THz beam is linearly

polarized with 99.5% purity (Extended Data Fig. 9). As the over-the-air (OTA) distance *D* increases, the transmission over the entire bandwidth decreases due to the increased free-space path loss[24] which can be compensated by using a higher-stage topological beamformer with enhanced gain (Figs. 4c and 4d).

The measured error vector magnitude (EVM) decreases linearly as the relative carrier signal power increases (Fig. 4e) due to the improved signal-to-noise ratio (SNR) and the enhanced channel performance. For 20 Gbit/s data rate using quadrature amplitude modulation (QAM)-16 with a carrier frequency f_c = 0.325 THz, the power penalty is close to the OTA total loss (Fig. 4c). It indicates that employing topological beamformers with higher gain or boosting transmitted power[25] to counteract free-space path loss enables directional signal transmission over long distances. As data rate rises, so does the required bandwidth, with increased loss near the transmission band edges resulting in greater power penalties. The clearly defined constellation points for topological beamformers showcase high-speed data (72 Gbit/s) and long-range (300 mm) THz wireless communications (Fig. 4f).

Eight 40 Gbit/s THz wireless links

Finally, we demonstrate eight 40 Gbit/s THz wireless communication links using an AB-type 4-stage topological beamformer emitting eight THz beams. The THz signal with a carrier frequency f_c = 0.332 THz is modulated through quadrature phase shift

keying (QPSK) phase modulation and QAM-16 (see Methods). Each THz beam enables a THz wireless link with 20 Gbit/s (QPSK modulation) or 40 Gbit/s (QAM-16) data speed (Fig. 4g), and hence the topological beamformer provides eight wireless links simultaneously. We further use four (links 5 to 8) of the eight links to demonstrate point-to-multipoint High-Definition Television (HDTV) streaming (Fig. 4h-(i) and Methods). When the receiver was rotated to the positions where the wireless links form, stable HDTV streaming was obtained (Fig. 4h-(ii)), while it was interrupted when the receiver was moved away from the wireless link positions (see Supplementary Videos SV2).

In conclusion, we demonstrated on-chip THz topological beamformers capable of providing full 360° azimuthal coverage. The topological valley vortices enable the robust waveguiding and splitting of THz waves and ensure channel isolation of the phased arrays. This results in low-loss, broadband and large-scale beamforming. Additionally, we achieved reconfigurable photoswitching and controlled the number of THz beams by photoexciting the silicon chip and modulating the on-chip THz signal. For real-time THz beamforming and beam steering, silicon topological beamformers can be integrated with micro-electromechanical systems (MEMS) to modulate the spatial phase profile using self-adaptive deep reinforcement learning. For instance, bimorph cantilever arms can be incorporated into the taper coupler of the topological beamformer, enabling active control of the radiation pattern by adjusting biasing voltages on the cantilever array (see Supplementary Section 11 for the details of

MEMS-integrated reconfigurable topological beamformer). Utilizing topological beamformers for highly directional THz wave transmission and reception, we achieved 72 Gbps chip-to-chip THz wireless communication over a distance of 300 mm. Furthermore, we demonstrated eight simultaneous 40 Gbps communication links and realized point-to-multipoint HDTV streaming with a single topological beamformer. Our study presents an ideal THz topological photonic integrated circuit platform, enabling low-loss, highly directional, and wideband THz beamforming for future 6G to XG SIMO and MIMO wireless communications.

References

1 Alsharif, M. H. & Nordin, R. Evolution towards fifth generation (5G) wireless networks: current trends and challenges in the deployment of millimetre wave, massive MIMO, and small cells. *Telecommun. Syst.* **64**, 617-637 (2017).

2 Dang, S., Amin, O., Shihada, B. & Alouini, M.-S. What should 6G be? *Nat. Electron.* **3**, 20-29 (2020).

3 Akyildiz, I. F., Kak, A. & Nie, S. 6G and beyond: the future of wireless communications systems. *IEEE Access* **8**, 133995-134030 (2020).

4 Rappaport, T. S. *et al.* Wireless communications and applications above 100 GHz: opportunities and challenges for 6G and beyond. *IEEE Access* **7**, 78729-78757 (2019).

5 Nagatsuma, T., Ducournau, G. & Renaud, C. C. Advances in terahertz communications accelerated by photonics. *Nat. Photonics* **10**, 371-379 (2016).

6 Akyildiz, I. F., Jornet, J. M. & Han, C. Terahertz band: next frontier for wireless communications. *Phys. Commun.* **12**, 16-32 (2014).

7 Koenig, S. *et al.* Wireless sub-THz communication system with high data rate. *Nat. Photonics* **7**, 977-981 (2013).

8 Fu, X., Yang, F., Liu, C., Wu, X. & Cui, T. J. Terahertz beam steering technologies: from phased arrays to field-programmable metasurfaces. *Adv. Opt. Mater.* **8**, 1900628 (2020).

9 Monnai, Y., Lu, X. & Sengupta, K. Terahertz beam steering: from fundamentals to applications. *J. Infrared, Millimeter, Terahertz Waves* **44**, 169-211 (2023).

10 Tan, Y. J. *et al.* Self-adaptive deep reinforcement learning for THz beamforming

with silicon metasurfaces in 6G communications. *Opt. Express* **30**, 27763-27779 (2022).

11 Sengupta, K. & Hajimiri, A. A 0.28 THz power-generation and beam-steering array in CMOS based on distributed active radiators. *IEEE J. Solid-State Circuits* **47**, 3013-3031 (2012).

12 Tousi, Y. & Afshari, E. A high-power and scalable 2-D phased array for terahertz CMOS integrated systems. *IEEE J. Solid-State Circuits* **50**, 597-609 (2015).

13 Che, M. *et al.* Optoelectronic THz-wave beam steering by arrayed photomixers with integrated antennas. *IEEE Photonics Technol. Lett.* **32**, 979-982 (2020).

14 Sengupta, K., Nagatsuma, T. & Mittleman, D. M. Terahertz integrated electronic and hybrid electronic–photonic systems. *Nat. Electron.* **1**, 622-635 (2018).

15 Zeng, Y. *et al.* Electrically pumped topological laser with valley edge modes. *Nature* **578**, 246-250 (2020).

16 Shalaev, M. I., Walasik, W., Tsukernik, A., Xu, Y. & Litchinitser, N. M. Robust topologically protected transport in photonic crystals at telecommunication wavelengths. *Nat. Nanotechnol.* **14**, 31-34 (2019).

17 Gao, F. *et al.* Topologically protected refraction of robust kink states in valley photonic crystals. *Nat. Phys.* **14**, 140-144 (2018).

18 Dong, J.-W., Chen, X.-D., Zhu, H., Wang, Y. & Zhang, X. Valley photonic crystals for control of spin and topology. *Nat. Mater.* **16**, 298-302 (2017).

19 Ma, T. & Shvets, G. All-Si valley-Hall photonic topological insulator. *New J. Phys.* **18**, 025012 (2016).

20 Yang, Y. *et al.* Terahertz topological photonics for on-chip communication. *Nat. Photonics* **14**, 446-451 (2020).

21 Kumar, A. *et al.* Phototunable chip-scale topological photonics: 160 Gbps waveguide and demultiplexer for THz 6G communication. *Nat. Commun.* **13**, 5404 (2022).

22 Jia, R. *et al.* Valley-conserved topological integrated antenna for 100-Gbps THz 6G wireless. *Sci. Adv.* **9**, eadi8500 (2023).

23 Hatsugai, Y. Edge states in the integer quantum Hall effect and the Riemann surface of the Bloch function. *Phys. Rev. B* **48**, 11851-11862 (1993).

24 Balanis, C. A. *Modern Antenna Handbook*. (John Wiley & Sons, 2011).

25 Sen, P., Siles, J. V., Thawdar, N. & Jornet, J. M. Multi-kilometre and multi-gigabit-per-second sub-terahertz communications for wireless backhaul applications. *Nat. Electron.* **6**, 164-175 (2023).

Main Figures

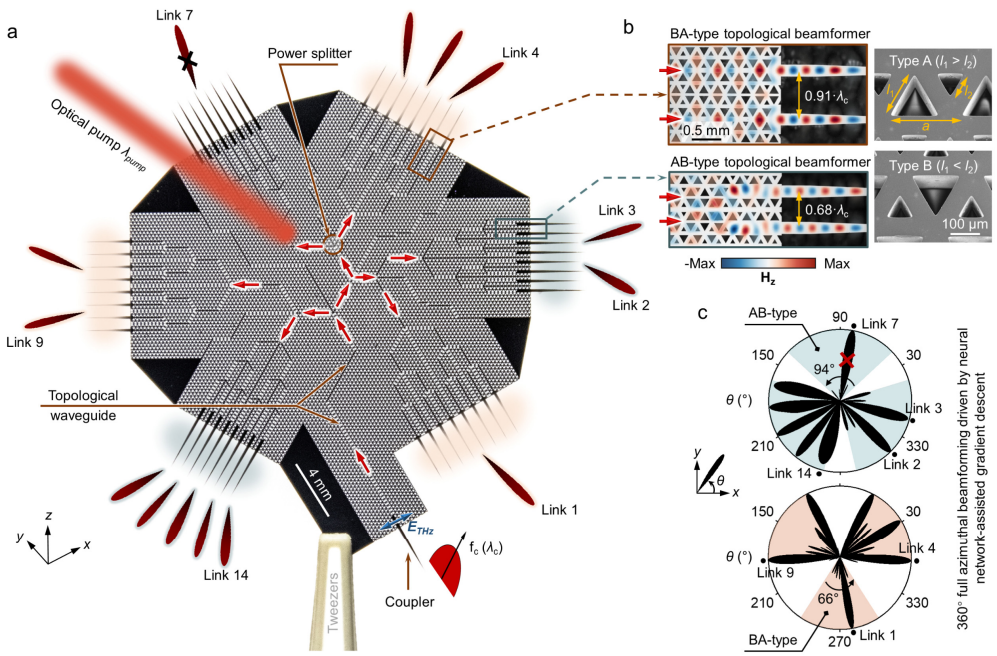

Fig. 1 | Multi-link THz topological beamformer silicon chip for 6G to XG wireless. a Optical image of the THz topological beamformer and the schematic of phototunable beamforming. The 360° topological beamformer features 184 valley-locked waveguides, 54 power splitters, and 136 sharp bends with a footprint of 3.5 cm × 3.2 cm. The THz signal with a carrier frequency f_c is coupled to the chip through a taper, then guided by the topological waveguides, split by the power splitters, channeled into six branches, and transmitted toward different directions in free space, providing multi-links simultaneously at arbitrary azimuthal angles. The radiation pattern is modulated by photoexciting the silicon topological chip to switch off the THz beam using an optical laser with wavelength λ_{pump} = 525 nm. **b** Optical images of the taper area of AB-type and BA-type topological beamformers. The superimposed colormap represents the simulated magnetic field distributions H_z. The distance between the neighboring channels of AB- and BA-type topological beamformers is 630 and 840 μm, respectively. Insets show the scanning electron microscopy (SEM) images of VPC unit cells which consist of two equilateral triangular air holes with a side length of l_1 and l_2, respectively. The lattice constant a = 242.5 μm. $l_1 = 0.65a > l_2 = 0.35a$ ($l_1 = 0.35a < l_2 = 0.65a$) in Type A (Type B) VPC unit cell. **c** Predicted far-field radiation patterns of the three branches of AB-type (upper panel) and BA-type (low panel) beamformers based on the neural network (NN)-assisted inverse design. Each AB- (BA-) type high-gain beamformer transmits the THz signal toward different directions with desired arbitrary azimuthal angles within a range of 94° (66°) considering f_c = 0.325 THz, which finally results in 360° full azimuthal beamforming with three AB and three BA sections on a single chip.

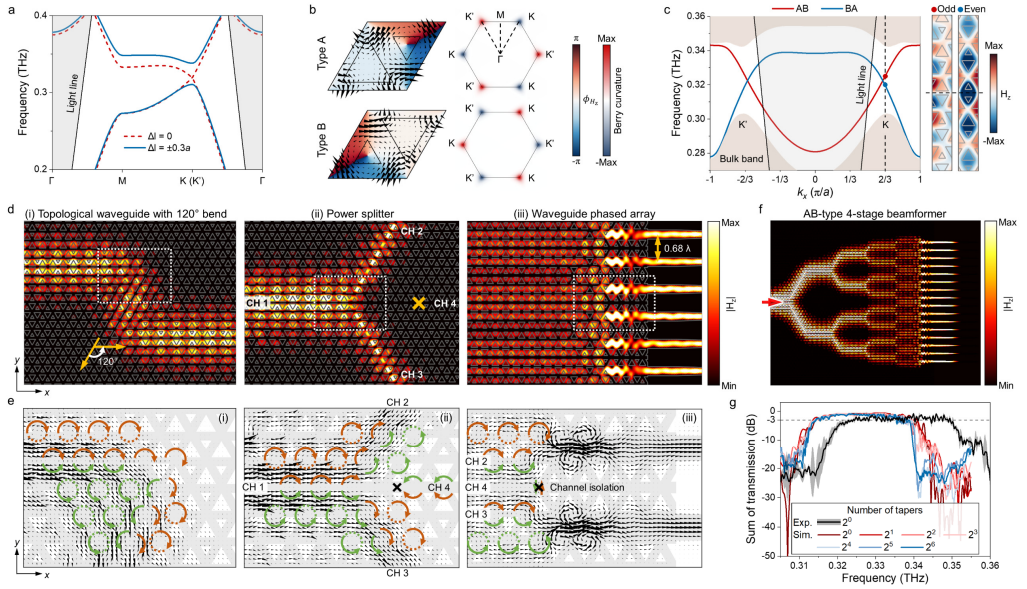

Fig. 2 | Topological valley vortices-driven robust guiding, power splitting, and channel isolation. a Calculated band structures of VPCs with ($\Delta l = l_1 - l_2 = 0$) and without ($\Delta l = \pm 0.3a$) inversion symmetry. **b** Calculated phase distribution of the magnetic field H_z and Berry curvature of the lower band for Type A and Type B VPC unit cells. The black arrows denote the Poynting vector flow. **c** The projected band diagram of AB-type (BA-type) zigzag interface where two large (small) triangular air holes face each other near the interface. The inset shows the calculated magnetic field profile H_z of the edge states supported in AB- and BA-type interfaces at K valley, exhibiting odd and even symmetry along the interface, respectively. Simulated **d** $|H_z|$ field distributions and **e** Poynting vector flow in the (i) AB-type topological waveguide having two sharp 120° bends, (ii) AB-type four-channel (4-CH) power splitter, and (iii) the taper area of AB-type topological waveguide phased array at 0.325 THz. The simulation areas in **e** are indicated by white dashed boxes in **d**. The brown (green) circles in **e** denote the clockwise (anti-clockwise) vortices in Type A (B) VPC unit cell at K valley. The dashed part of the circles undergoes destructive interference with the neighboring vortex which is closer to the interface and has stronger and opposite Poynting vector flow. **f** Simulated magnetic field distribution $|H_z|$ of the AB-type 4-stage topological beamformer at 0.325 THz. The input THz signal on the left side is equally split into 16 channels and radiated into free space through tapers. **g** Simulated and measured transmission of AB-type topological beamformers having different number of tapers by summing the transmission of all the channels. The shaded gray area of the measured transmission spectrum indicates the standard error.

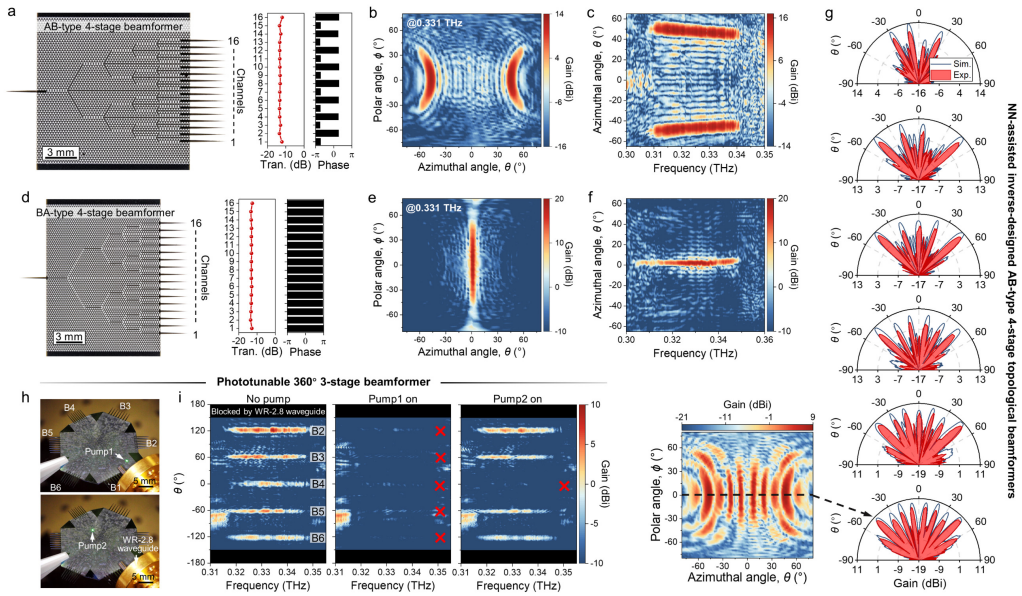

Fig. 3 | Intrinsic and NN-assisted inverse-designed topological beamformers. a (**d**) Optical image of intrinsic AB- (BA-) type 4-stage topological beamformer silicon chip with 16 radiating channels. Inset of **a** (**d**) shows the simulated transmission and phase of all the 16 channels at 0.325 (0.32) THz. Measured 3D radiation pattern of intrinsic **b** AB-type and **e** BA-type 4-stage topological beamformers at 0.331 THz. Measured broadband radiation pattern of intrinsic **c** AB-type and **f** BA-type 4-stage topological beamformers. **g** Measured and simulated radiation patterns of AB-type 4-stage topological beamformers having different spatial profiles of taper length, which is inverse-designed via NN-assisted gradient descent. Three to eight beams covering a wide azimuthal angle range of 91.8° are demonstrated at 0.331 THz. The inset shows the measured 3D radiation pattern of the topological beamformer with 8 beams. **h** Optical images of the fabricated 360° topological beamformer having six branches (B1 to B6). The topological chip is photoexcited by a 525 nm continuous wave laser (diameter of the beam spot = 0.55 mm, pump fluence = 902.9 W/cm^2) at the main domain wall before any intersection (Pump1) or at the domain wall before branch B4 (Pump2). **i** Measured broadband radiation patterns of the 360° topological beamformer without optical pump, with Pump1 on, and with Pump2 on. The radiation in the large azimuthal angles (from -180° to -150° and from 150° to 180°) is blocked by the WR-2.8 waveguide which is used to couple the THz wave into the chip.

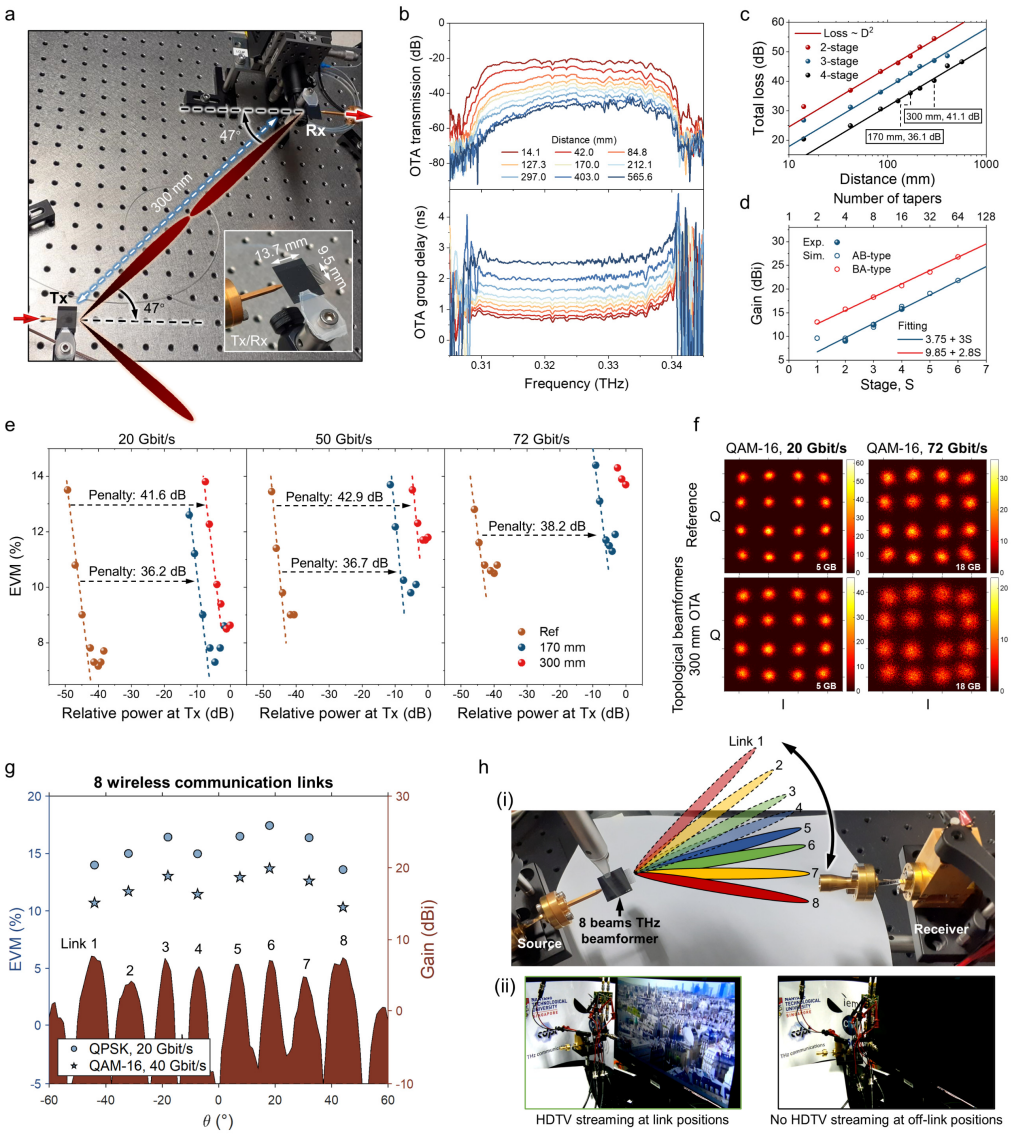

Fig. 4 | THz wireless communication with eight 40 Gbit/s links and point-to-multipoint HDTV streaming. a Experimental setup of the chip-to-chip THz wireless communications. The intrinsic AB-type 4-stage topological beamformers are used as both transmitter (Tx) and receiver (Rx). Inset shows the topological beamformer. **b** Measured transmission and group delay spectra over-the-air (OTA) between the Tx and Rx for different distances. **c** Measured total loss between two AB-type 2, 3, and 4-stage topological beamformers at 0.325 THz for different distances. **d** Measured and simulated gain of different stage intrinsic AB- and BA-type topological beamformers. **e** Measured error vector magnitude (EVM) versus relative power at the Tx recorded at 20, 50, and 72 Gbit/s for the topological beamformers separated by 170 and 300 mm. The measurements were compared with the reference measurements where the topological chip was not used, and the Tx and Rx waveguides were directly in contact. **f** Measured I-Q constellation diagram corresponding to 20 and 72 Gbit/s using quadrature amplitude modulation (QAM)-16 with 5 and 18 GBaud symbol rate through the reference

(without the chip) and topological beamformers separated by 300 mm. **g** Measured EVM of the AB-type 4-stage topological beamformer for data rates of 20 Gbit/s (quadrature phase shift keying (QPSK) modulation) and 40 Gbit/s (QAM-16) with a carrier frequency of 0.332 THz. The measured gain of the topological beamformer shows that it has eight radiating beams, each of which provides a THz wireless link. **h-(i)** Experimental setup of point-to-multipoint High-Definition Television (HDTV) streaming over 100 mm. **h-(ii)** Real-time HDTV streaming when the receiver was moved to the azimuth angles of 7.5°, 18°, 32°, and 44°. It was interrupted when the receiver was moved away from the wireless link positions.

Methods

Topological beamformer chip fabrication

The VPC beamformer chip was fabricated using high-resistivity (>10 kΩ·cm) silicon wafer. The 2, 3, and 4-stage intrinsic AB-type topological beamformers were fabricated using 250 μm thick silicon wafers while all the other samples were fabricated using 215 μm thick silicon wafers. The variation in the thickness of silicon wafer caused the frequency shift of the transmission band (Supplementary Section 6). To fabricate the topological devices, a 2 μm thick silicon dioxide (SiO_2) thin film was first deposited as an etching protective mask. The VPC design was patterned on the SiO_2 layer using conventional UV photolithography process followed by reactive ion etching (RIE). The remaining pattern of SiO_2 layer works as a protective mask and the silicon wafer was then etched through using deep reactive ion etching (DRIE, Oxford Estrelas).

Numerical simulation

The eigenmode analysis, including calculating the band structure of the VPC unit cell and edge states of topological interfaces, was performed using the eigenvalue solver of

the commercial software COMSOL Multiphysics. The dielectric constant was set as 1 and 11.7 for air and silicon, respectively. Floquet boundary conditions were applied in both x and y directions in the VPC unit cell and at only x directions in the topological interfaces. The transmission and far-field radiation pattern of the topological beamformers were calculated using the time domain solver of the commercial software CST Studio Suite. The materials were defined as the same as in the eigenmode calculations. Waveguide ports were used to excite the edge states of the topological interfaces and to calculate the transmission of the topological beamformer. 3D far-field monitors were used to calculate the radiation pattern.

Experimental setup

On-chip THz transmission characterization setup

The on-chip transmission of the fabricated 0-stage AB-type and BA-type topological beamformers which have only one output channel was characterized using a set of Virginia Diodes Inc (VDI) frequency extension modules (Supplementary Section 5). A microwave signal ranging from 250 kHz - 20 GHz was first generated by Keysight PSG Analog Signal Generator and then upconverted by the VDI spectrum generator extension module (WR2.8SGX, 260 GHz - 400 GHz). The up-converted THz signal was coupled with the taper and fed into the VPC chip through a WR-2.8 metallic hollow waveguide. The output signal was collected by another WR-2.8 waveguide, down-converted with VDI spectrum analyzer extension module (WR2.8SAX, 260 GHz - 400

GHz), and finally analyzed by Keysight EXA Signal Analyzer. The transmission of the VPC chips were obtained by normalizing the measured signal with the reference signal where the two WR-2.8 waveguides were connected directly. The measured transmission was averaged over ten measurements from two identical samples fabricated on the same wafer. Since the dimension of the WR-2.8 waveguide (diameter is 19.05 mm) was much larger than the gap (0.63 mm for AB-type and 0.84 mm for BA-type beamformer) between the neighboring tapers of the beamformers, the transmission of n-stage ($n \geq 1$) topological beamformers having 2^n tapers was not measured.

Over-the-air (OTA) THz transmission and group delay characterization setup

The vector network analyzer (VNA) setup was used to characterize the OTA transmission and group delay of the topological beamformers. The VNA system consisted of a pair of frequency extenders (Z-325 and Z-500 type) driven by a ZVA-24 from Rohde & Schwarz, in the WR-3.4 and WR-2.2 waveguide configuration to cover the entire frequency band of interest for the beamformers, falling in both 220-325 GHz and 325-500 GHz bands. The system was first waveguide calibrated using a TRM (Thru, Reflect, Match) waveguide calibration procedure as per WR-3.4 or WR-2.2 waveguide standards. After calibration, the transmission was 1 (0 dB) and the group delay which represents the time taken for the signal to travel through the device under test was 0. Then, the WR-3.4 or WR-2.2 waveguides which were used to couple in and out the THz signal to the VPC chip were measured alone in a “back-to-back” configuration, in

which a pair of the waveguides were connected directly to each other. This reference signal measured the transmission and group delay of the waveguides only. Finally, the transmission and group delay between the VPC chips separated at different distances over the air (OTA) were measured in a symmetric configuration where a pair of VPC chips were coupled to the waveguides at both Tx and Rx. The relative OTA transmission and group delay of the VPC chips were obtained by subtracting the reference signal.

THz radiation pattern characterization setup

The radiation pattern of the VPC beamformers was characterized using a similar setup of the on-chip THz transmission measurements. Instead of using a WR-2.8 waveguide to collect the output signal, the radiated THz beam was received by a WR-2.8 diagonal horn antenna, placed 200 mm away at a motor-driven rotational stage covering the azimuthal angle from -150° to 150° (Supplementary Section 5).

THz communication experiment setup

Two different experimental THz communication setups were used to characterize the wireless communication performance of the beamformers. The first one was dedicated to I/Q modulations, while the second one enabled real-time streaming of High-Definition Television (HDTV). In the first setup, two tunable lasers were used to generate a dual-tone signal in the optical domain with 331 GHz frequency shifts. One of the tone signals was modulated by an I/Q Mach-Zehnder $LiNbO_3$ modulator. The I

484 and Q data streams were generated by a Keysight M8195A arbitrary waveform
485 generator. An optical amplification stage was used to set the appropriate optical power
486 to be sent inside the optical-to-THz converter (photomixer). The photomixer comprised
487 of unitravelling-carrier-photodiode (UTC-PD) with waveguide output. The 331 GHz
488 signal was further coupled to topological beamformer devices by inserting the silicon
489 coupler taper into the hollow-core metallic waveguide which was connected to the
490 UTC-PD output. A waveguide heterodyne receiver was used, which composed of a
491 GaAs Schottky-barrier sub-harmonic mixer coupled to a local oscillator at 150 GHz.
492 The intermediate frequency (IF) signal (coaxial mixer output) was amplified with a
493 distributed amplifier (SHF810) to further feed a wideband real-time oscilloscope (UXR
494 70 GHz from Keysight). The detected signal was finally analyzed using off-line signal
495 processing composed of equalization to compensate for the received signal. The output
496 parameters of the off-line analysis consisted of the signal-to-noise ratio (SNR),
497 constellation diagrams, eye diagrams, and error-vector magnitude (EVM).
498
499 The second setup used an HDMI-to-serial data interface (SDI) converter to encode the
500 video stream onto the two laser tones using a second Mach-Zehnder modulator, which
501 was optimized for amplitude modulation. In this case, the data rate was fixed by the
502 HDTV stream (1920×1024 pixels resolution, which corresponded to 1.5 Gbit/s). The
503 same UTC-PD and waveguides were used to couple the modulated THz data to the
504 beamformer. The transmitted THz signal over a distance of 100 mm was received and

fed to an amplified direct-detection (envelope detection) receiver at 331 GHz. Envelope detection enabled baseband (binary) data detection in real-time, i.e., without any signal processing nor off-line process. The output binary data was then fed to an SDI-to-HDMI converter, then displayed on a TV. The receiver was mounted on an automated rotation stage to sweep different spatial locations. Real-time video transmission was obtained at expected locations using the 8-beam beamformer (See Supplementary Videos SV2).

Reconfigurable 360° topological beamformer

The reconfigurable photoswitching and controlling the number of beams in the 360° topological beamformer was investigated by photoexciting the silicon VPC chip at different positions with a continuous wave laser of wavelength 525 nm (E = 2.36 eV). The optical beam was focused to a small spot (diameter of the beam spot = 0.55 mm, pump fluence = 902.9 W/cm^2) to ensure uniform illumination of few VPC unit cells. As shown in Extended Data Fig. 7, when the VPC chip was pumped at positions P1~P5, the THz beams radiated by the B2~B6 branches were switched off one by one with a gain modulation ≥ 8.3 dB. Alternatively, when the topological chip was pumped at positions before the power splitter, two (pump at P6, P7, and P8), four (pump at P9), or all six (pump at P10) beams were switched off simultaneously. The pump position-dependent photoswitching and the control of the number of THz beams are summarized in Extended Data Table. 1. Furthermore, the topological beamformer was pumped at

position P1 with different pump fluences. As shown in Extended Data Fig. 8a, when the pump fluence increases, the gain of the broadband THz beam radiated by the B2 branch decreases. A large change of gain 16.3 dBi was obtained at a pump fluence 902.9 W/cm^2 compared to a no-pump case (Extended Data Fig. 8b).

Acknowledgements

Authors acknowledge the research funding support from National Research Foundation (NRF) Singapore, Grant No: NRF-CRP23-2019-0005 (TERACOMM). G.D. and P.S. state that the characterization testbeds are supported by France 2030 programs, PEPR (Programmes et Equipements Prioritaires pour la Recherche) and CPER Wavetech. The PEPR is operated by the Agence Nationale de la Recherche (ANR), under the grants ANR-22-PEEL-0006 (FUNTERA, PEPR 'Electronics') and ANR-22-PEFT-0006 (NF-SYSTERA, PEPR 5G and beyond - Future Networks). The Contrat de Plan Etat-Region (CPER) WaveTech is supported by the Ministry of Higher Education and Research, the Hauts-de-France Regional council, the Lille European Metropolis (MEL), the Institute of Physics of the French National Centre for Scientific Research (CNRS) and the European Regional Development Fund (ERDF).

Author contributions

W.W. and R.S. conceived the idea. W.W., Y.J.T., A.K. and R.S. designed the experiments. W.W. performed the simulation. Y.J.T. performed the neural network-

assisted inverse design of the topological beamformers. P.P. fabricated a portion of the intrinsic AB-type topological beamformer samples and T.C.T. led the overall sample fabrication. W.W. performed the on-chip transmission and 2D radiation pattern measurements with the help of T.C.T. W.W. and R.S. designed the phototunable beamforming experiment and W.W. performed the active tuning measurements with the help of T.C.T. G.D. performed the VNA transmission, antenna gain and 3D radiation pattern measurements. P.S. and G.D. performed THz wireless communication experiments. W.W., Y.J.T., A.K., G.D. and R.S. analyzed all the data. W.W. and R.S. wrote the manuscript with inputs from all co-authors. R.S. led the overall project.

Competing interests

The authors declare no competing interests.

Correspondence and requests for materials should be addressed to Ranjan Singh (ranjans@ntu.edu.sg).

Data availability

All the data in this study are openly available in NTU research data repository DR-NTU at https://doi.org/10.21979/N9/UKLX3D.

Extended Data

Extended Data Table

Extended Data Table 1. Reconfigurable photoswitching and control over the number of THz beams in the 360° topological beamformer at different pump positions P1-P10.

	B1[a]	B2	B3	B4	B5	B6
No Pump	√[b]	√	√	√	√	√
P1[c]	√	× (11.9 dB)[d]	√	√	√	√
P2	√	√	× (12.3 dB)	√	√	√
P3	√	√	√	× (9.6 dB)	√	√
P4	√	√	√	√	× (9.3 dB)	√
P5	√	√	√	√	√	× (8.3 dB)
P6	√	× (13.1 dB)	× (11.1 dB)	√	√	√
P7	√	√	√	× (5.8 dB)	× (8.5 dB)	√
P8	×	√	√	√	√	× (8.0 dB)
P9	×	√	√	× (5.9 dB)	× (10.8 dB)	× (10.6 dB)
P10	×	× (14.6 dB)	× (13.6 dB)	× (10.0 dB)	× (9.4 dB)	× (10.4 dB)

√ represents "ON" state and × represents "OFF" state.

[a] B1~B6 indicates the THz beams radiated by the branches B1~B6.

[b] The THz beam radiated by branch B1 is blocked by the WR-2.8 waveguide.

[c] See Extended Data Fig. 7 for the details of the pump positions P1-P10.

[d] 11.9 dB denotes the changes in the maximum gain of the "ON" (no pump) and "OFF" states. See Extended Data Fig. 8 for the detailed discussion about the effect of pump fluence on the gain of THz beams.

Extended Data Figure

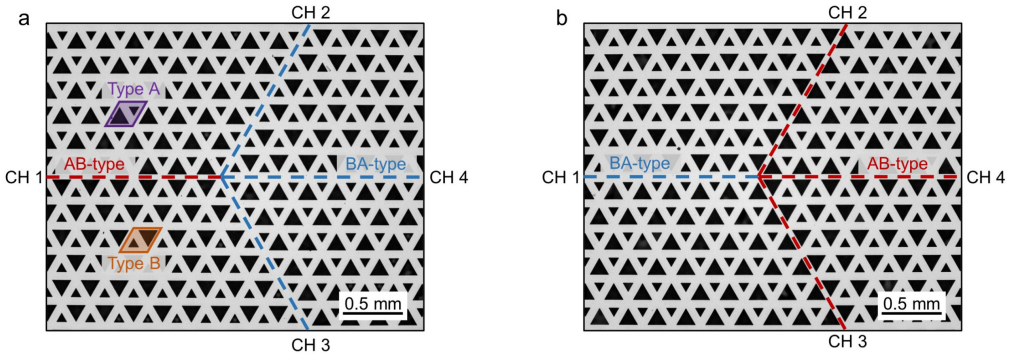

Extended Data Fig. 1 | Topological power splitters. Optical images of four-channel (4-CH) **a** AB-type and **b** BA-type topological power splitters. Type A (B) VCP unit cell is highlighted with a purple (orange) color. The AB-type and BA-type zigzag interfaces are marked with red and blue dotted lines, respectively. The 4-CH AB-type (BA-type) power splitter is composed

of an AB-type (BA-type) zigzag interface on the left channel CH 1 and three BA-type (AB-type) zigzag interfaces on the right channels CHs 2-4.

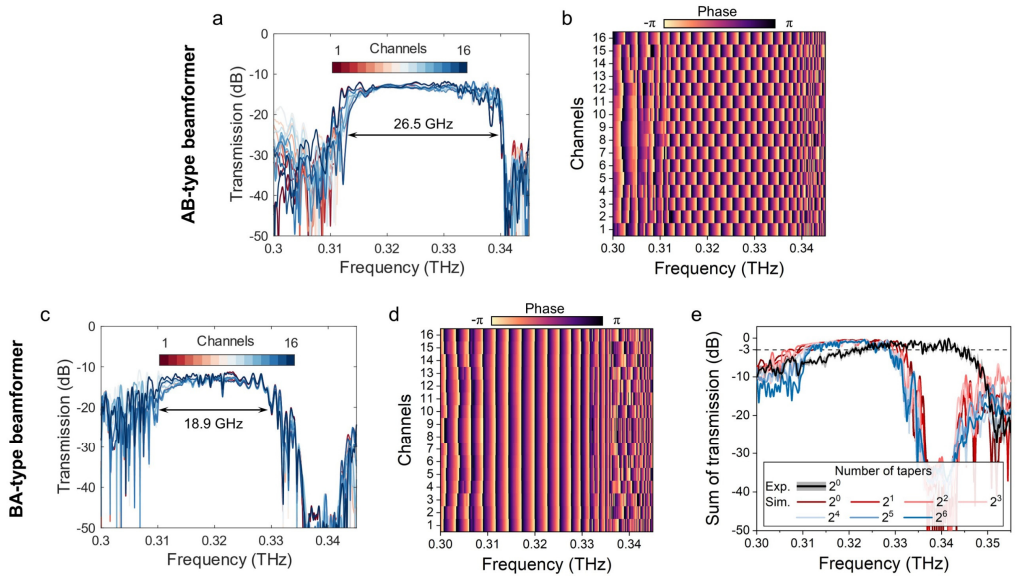

Extended Data Fig. 2 | Intrinsic broadband topological waveguide phased arrays. Simulated **a** (**c**) transmission and **b** (**d**) phase of the 16 radiating channels of AB- (BA-) type 4-stage topological beamformer. The 16 channels of AB- (BA-) type beamformer have similar transmission while showing intrinsic π (0) phase difference between adjacent channels over the entire broad bandwidth of 26.5 GHz (18.9 GHz). **e** Simulated and measured transmission of BA-type topological beamformers having different number of tapers by summing the transmission of all the channels. The shaded gray area of the measured transmission spectrum indicates the standard error.

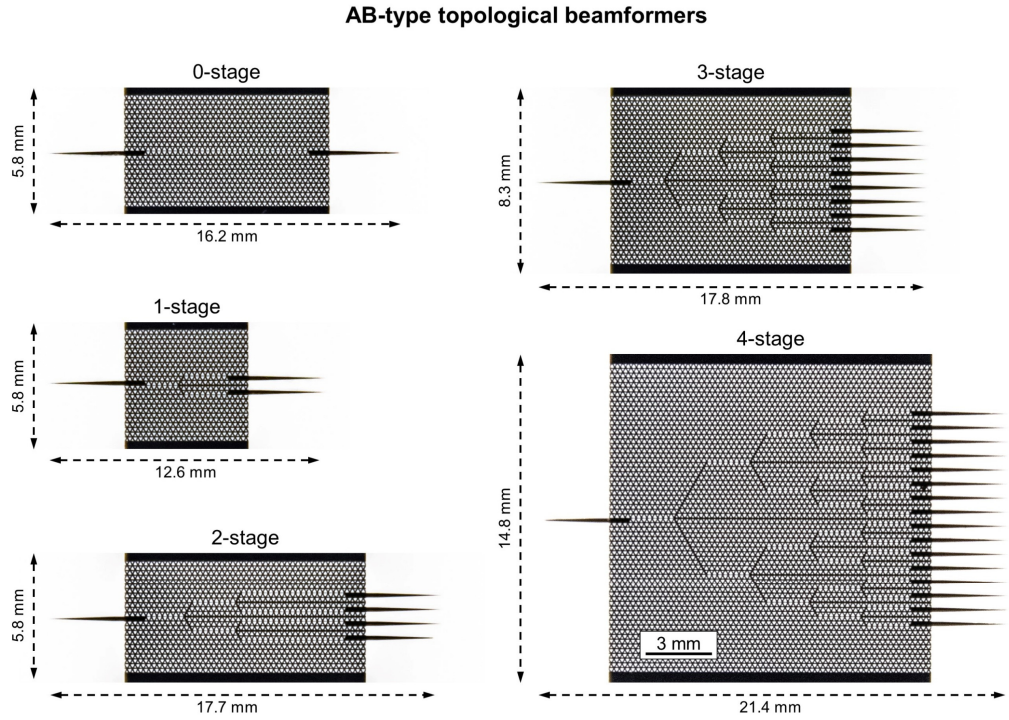

598

599 **Extended Data Fig. 3 | Optical images of AB-type topological beamformers.** The optical
600 images show the evolution of the AB-type topological beamformers from the 0-stage having 2^0
601 = 1 output taper to 4-stage having 2^4 = 16 output tapers.
602

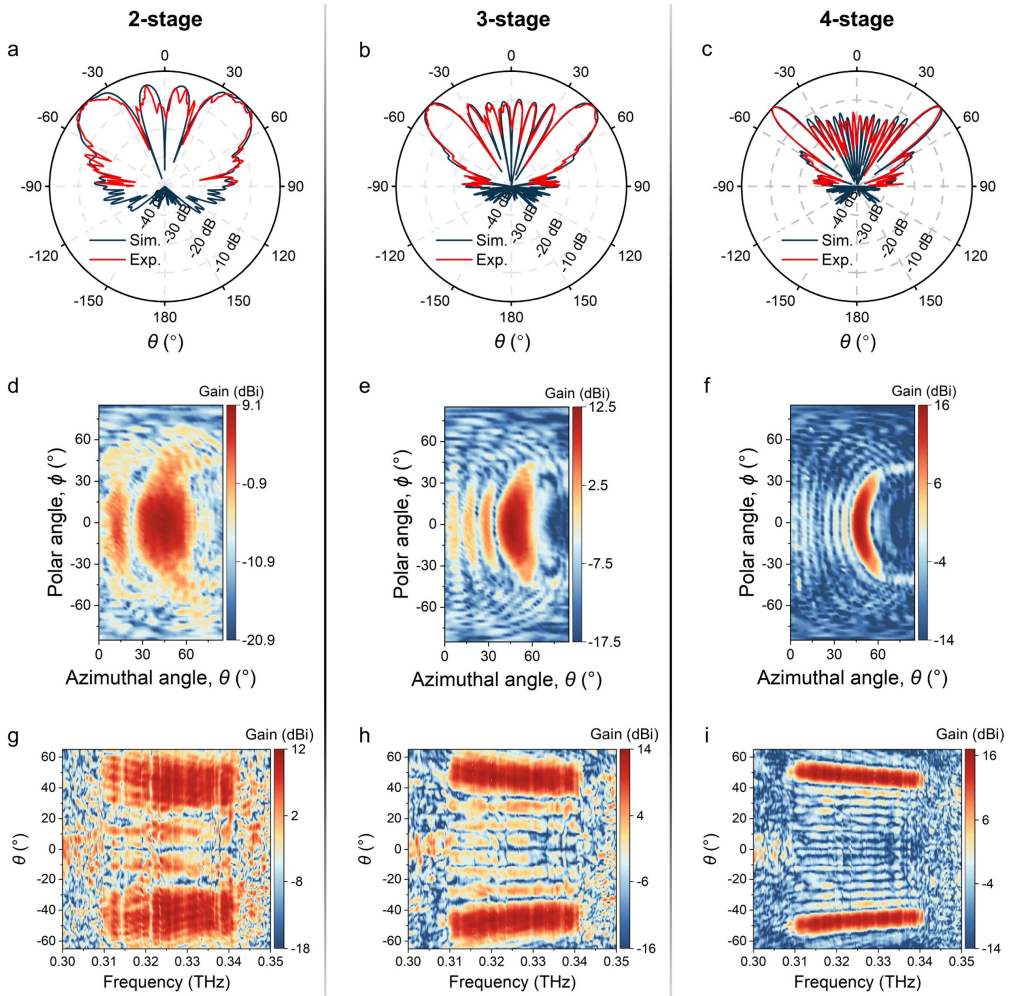

Extended Data Fig. 4 | Evolution of the far-field radiation pattern of intrinsic AB-type topological beamformer with the stage number. a,b,c Measured and simulated azimuthal radiation pattern of the intrinsic AB-type 2, 3, and 4-stage topological beamformers at the horizontal plane (polar angle ϕ = 0°) at 0.325 THz. **d,e,f** Measured 3D radiation patterns at 0.325 THz for the space $\theta > 0°$. **g,h,i** Measured broadband radiation pattern. As the number of taper (radiating channel) increases from 2^2 to 2^4, the gain of the main lobe increases from 12 to 16 dBi.

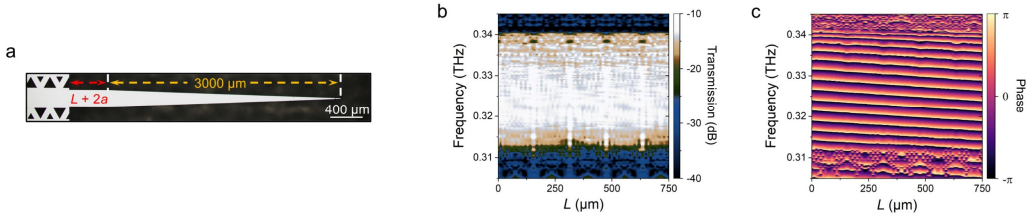

Extended Data Fig. 5 | Broadband 2π-phase control of topological beamformer's radiating channel. a Optical image of the taper region of the AB-type 4-stage topological beamformer. Simulated **b** transmission and **c** phase of a single taper of the AB-type 4-stage topological

beamformer as a function of frequency and length L of the rectangular bar of the taper coupler. The transmission remains constant, while the phase undergoes a 2π variation across the entire bandwidth.

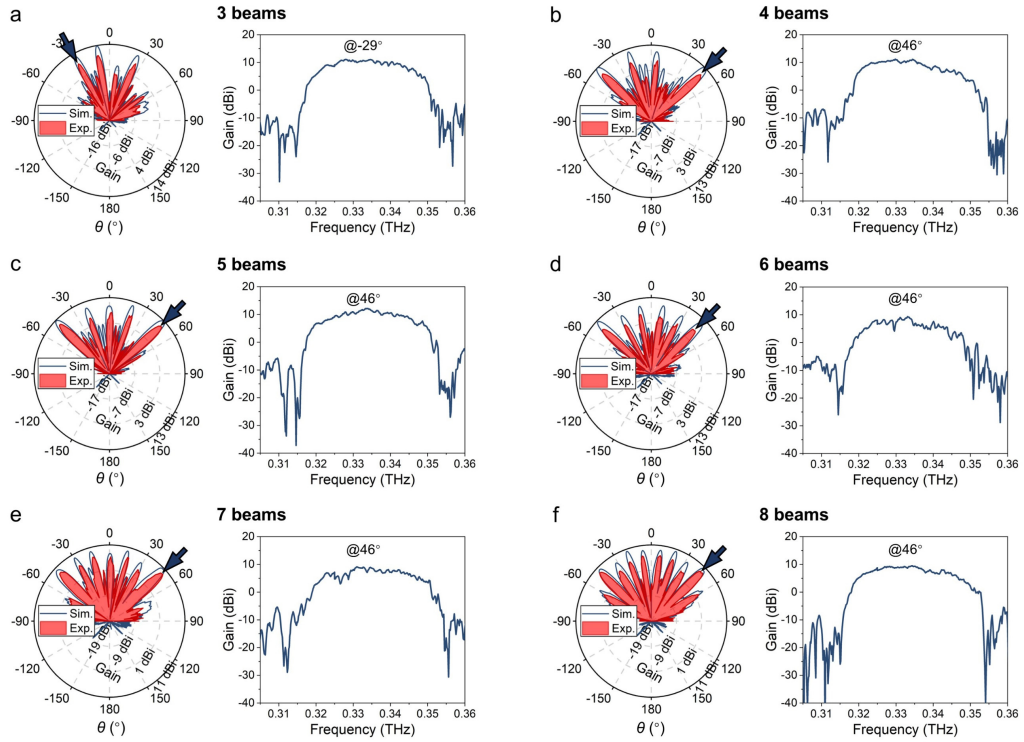

Extended Data Fig. 6 | Broadband beamforming with three to eight beams. a-f Measured and simulated radiation patterns at 0.331 THz (left panel) and measured broadband gain distribution (right panel) of the AB-type 4-stage topological beamformers having three to eight radiating beams. The arrows in the left panel of **a-f** indicate the azimuthal angle position where the gain is measured in the right panel.

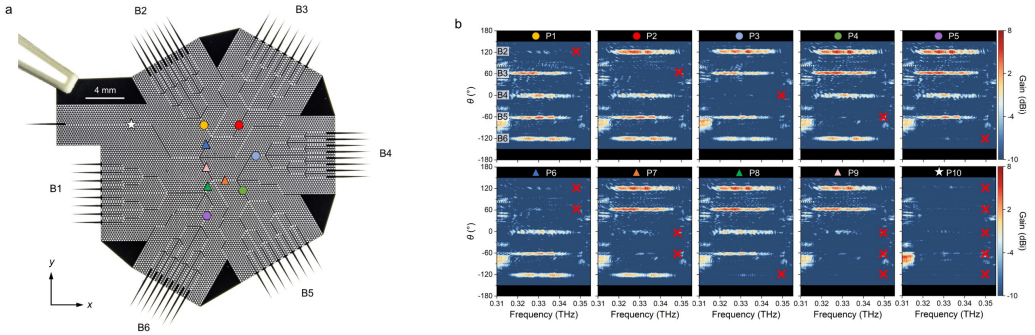

Extended Data Fig. 7 | Reconfigurable photoswitching and control of the number of THz beams in 360° topological beamformer. a Optical image of the 360° topological beamformer having six branches B1~B6. Each of the six branches transmits the THz signal into free space with a single radiated beam directed towards θ_B. Here θ_B = -120°, -60°, 0°, 60°, 120°, 180° is

the orientation azimuthal angle of each branch. The ten markers centered at the domain wall denote the pump positions of a 525 nm continuous wave laser (diameter of the beam spot = 0.55 mm, pump power fluence = 902.9 W/cm^2). **b** Measured broadband radiation patterns of the 360° topological beamformer pumped at different positions P1~P10.

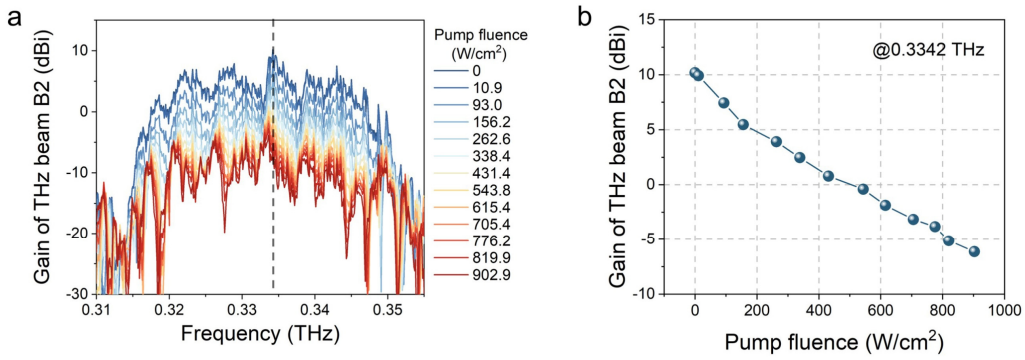

Extended Data Fig. 8 | Effect of pump fluence on the gain of topological beamformer. a Measured gain of the THz beam radiated by the B2 branch of the 360° topological beamformer at different pump fluences. The topological beamformer is pumped at position P1 marked by a yellow circle in Extended Data Fig. 7a. **b** Measured gain at 0.3342 THz which is indicated by a dashed line in **a**.

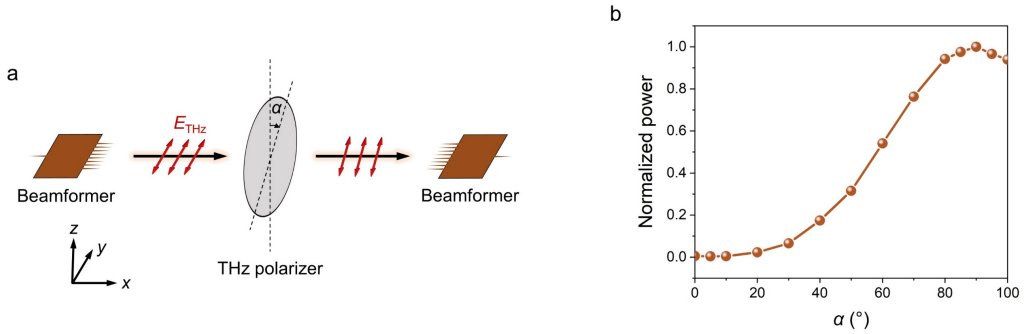

Extended Data Fig. 9 | Polarization analysis of topological beamformer. a Schematic of the experimental configuration for polarization analysis. The THz wave radiated by the topological beamformer passes through a THz polarizer in free space and then is received by another topological beamformer. The THz polarizer is a wire grid polarizer consisting of an array of metal wires on a High-Density Polyethylene (HDPE) film. Such polarizers have > 95% transmission in the 300 GHz band which is the frequency range of interest in this work. The diameter of the available surface is 40 mm, and it is POL-HDPE-CA40-OD50.8-T8 from TYDEX optics. **b** Normalized OTA transmittance for different polarization angle α at 0.325 THz. Maximum power is received at α = 90° and a minimum power of 0.005 is reached at α = 0°. It indicates that the THz beam radiated from the topological beamformer is highly TE-polarized with a polarization purity of 99.5%.